Proceedings of ASME Turbo Expo 2026
Turbomachinery Technical Conference and Exposition
GT2026
June 15-19, 2026, Milan, Italy
GT2026-176156

TIME-HISTORY STATISTICS OF SOOT FORMATION IN A MODEL GAS TURBINE COMBUSTOR

Kenji Miki[1], Francisco J. Guzman[1], Kumud Ajmani[1,2]

[1]NASA Glenn Research Center, Cleveland, OH, USA
[2]HX5 LLC, Cleveland, OH, USA

ABSTRACT

Soot formation is a complex dynamic and intermittent process determined by properties of the fuel, combustor design, and combustor operation. Although the major steps in soot formation (i.e., formation of precursors, inception, growth and evolution) are similar for a variety of carbonaceous fuels, applications, and operating conditions, it remains unclear when the temporal transition between these steps occurs. An engineering prediction tool coupled with computational fluid physics (CFD), therefore needs to accurately model all these complex steps of soot formation. To develop such a soot modeling tool, we propose a time-history concept to better understand the time dependency of soot formation as a function of local properties (i.e., temperature, velocity, local fuel air ratio, turbulence quantities etc.). We continue our previous work of modeling the DLR aero-combustor [1] with a semi-empirical two-equation soot model by injecting massless tracer particles upstream of the injector region of the combustor to collect time-history statistics of the solution variables. The computed correlations between the statistics of certain species with respect to the experimental soot volume fraction data showed that a time-history effect of certain flow variables, including turbulent kinetic energy, and multiple species is indeed important for soot formation. The time-history based correlation analysis was used to identify four key species and their respective concentration ranges deemed critical to improve the soot prediction of the current semi-empirical soot model (C_6H_5-based nucleation, acetylene-based surface growth, and oxidation with OH and O_2). A novel statistical time-history correlation coefficient concept is developed in this work to identify deficiencies and propose areas of improvement in an existing semi-empirical soot model.

Keywords: Emissions, Aircraft Engines, Soot Modeling

NOMENCLATURE

AoI	area of interest
BMMSM	bivariate multi-moment sectional method
CC	correlation coefficient (pearson correlation)
CFD	computational fluid dynamics
CQMOM	conditional quadrature methods of moments
C_a	agglomeration rate constant (=3)
DLR	the German Aerospace Center
DQMOM	direct quadrature methods of moments
FGM	flamelet-generated manifold
$f(p)$	functional dependence of soot surface growth
HMOM	hybrid method of moments
IRZ	inner recirculation zone
LES	large eddy simulation
MOM	method of moments
MOMIC	method of moments with interpolative closure
MTS-FPV	multi-time scale flamelet progress variable
N	soot number density
NDF	number density function
NOx	nitrogen oxides
N_t	threshold of particle number
ORZ	outer recirculation zone
PAH	polyaromatic hydrocarbon
PSDF	particle size distribution function
PVC	precessing vortex core
Δr_{inj}	radial length of particle injection region
S_1, S_2, S_3	rates of nucleation, surface growth and oxidation of soot
SVF	soot volume fraction
SND	soot number density
T	temperature
τ	particle-based averaged residence time
Δt	residence time in the AoI
TCSIs	turbulence-chemistry-soot interactions
THCC	time-history correlation coefficient (pearson correlation)
TKE	turbulence kinetic energy
u_i	velocity component
V_z	variance of mixture fraction
Δx_{inj}	axial location of particle injection
Y_i	i^{th} species mole fraction
$\overline{Y}_p$	mean progress variable
$\overline{Z}$	mean mixture fraction
Δz	length of pixel box in the normal direction
ϕ	equivalence ratio

INTRODUCTION

Soot is associated with adverse health effects [2] and is an indicator of combustion inefficiency. Ultra fine particle emissions, such as those emitted by gas turbines, can cause adverse pulmonary effects and be further transported to other interal organs by penetrating the body's air-blood barrier[3]. For gas turbines, soot can cause pitting of the turbine blades, clogging of the fuel injectors, and an increase in combustor cooling requirements [4]. Soot and thermal radiation are closely coupled [5] which can in turn change the temperature distribution and can have implications on the combustor's durability and the combustion efficiency [6]. Soot formation is a temporal and spatial dependent process determined by the properties of the fuel and combustion environment. Time-resolved studies of a model aero combustor [7-11] have shown that soot formation is an intermittent process governed by the unsteady mixing of distinct pockets of burned gases interchanging between rich and lean regions. Turbulent flame measurements [12, 13] and numerical studies [14-16] have similarly shown that soot formation is an intermittent process with distinct regions of inception, oxidation, and turbulent mixing. Studies on the spatial dependence of soot formation have shown that different parts of the flame are dominated by distinct chemical-growth pathways [12, 17-19].

Irrespective of the combustion environment, soot formation and subsequent evolution goes through the same key steps which include inception, fine-structure evolution, agglomeration, and aggregation [20]. Underlying the processes of soot formation and evolution is an inherent time dependency. Across different combustion systems (*i.e.,* laminar diffusion flames, turbulent non-premixed flames, aero combustors, etc.) a key difference is the time that the reactive mixtures spend at each of the soot formation and evolution steps. The evolution of the reactive mixture is a function of the local conditions (*i.e*., rich vs lean, temperature, chemical species available) and how much time is spent at these conditions. Although the key formation and evolution steps are the same for any combustion system, there is no clear cut-off or transition time between the steps [20]. Soot formation therefore has an inherent "time-history" or "memory" effect which is the result of the evolution of the distinct pockets of reactive mixtures. Evidence of the time-history effect on soot formation can be seen across several studies. Early studies investigated the early history of soot formation in a diffusion flame [21]. The authors observed that the structure of the soot changed with increasing burner height (*i.e.,* increasing flame residence time). For this simple flame, their analysis showed an increase in the aromatic content with increasing flame residence time. For turbulent cases, such as aero-combustors, time-history soot measurements are rare and very challenging since distinct packets of reacting gases must be tracked throughout the flame. The DLR model aero-combustor (see Fig. 1) is one such case with time-resolved soot measurements [7] including measurement of the temporal dynamics of the large-scale vortex structures on fuel-air mixing and their combined effects on soot formation [8].

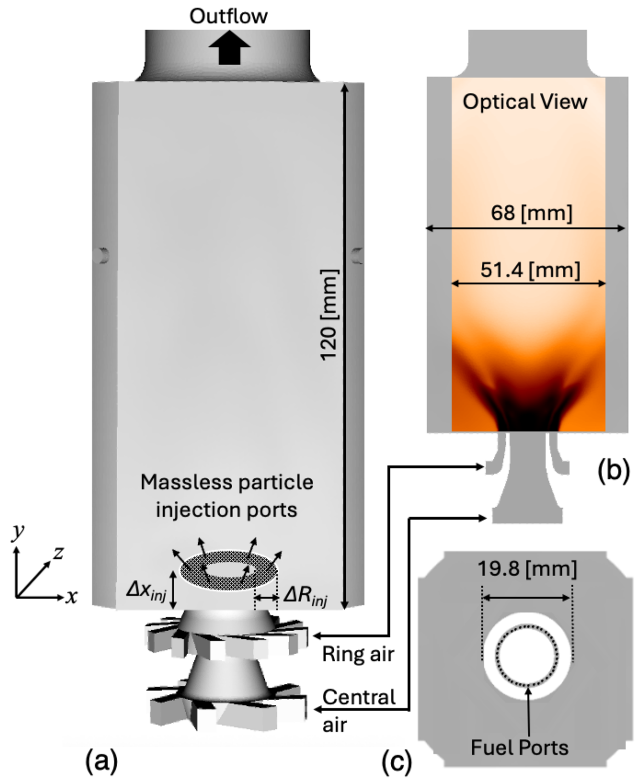

FIGURE 1: DLR EXPERIMENTAL SETUP FOR AN ETHYLENE AIR MODEL GAS TURBINE COMBUSTOR [1]

To properly predict soot formation a numerical soot model therefore has to capture the underlying physical process at the sub-grid scale. Briefly, we highlight some of the key numerical approaches used and their limitations. The numerical modeling of soot involves two general approaches, semi-empirical precursor models and detailed models solving for the particle size distribution function (PSDF) and number density function (NDF) [22, 23]. Semi-empirical precursor models, such as the two-equation Lindstedt model [24], are computationally inexpensive approaches that relate soot to precursor species via empirical kinetics coupled with chemistry including fuel decomposition steps, oxidation, and aromatic carbon species formation. Semi-empirical models solve for the soot mass fraction and soot number density scalars, but do not solve for the distribution functions. Detailed models try to solve for the distribution functions via an approximation of the population balance equation (PBE), but at an increased computational cost. Furthermore, since the PBE cannot be solved exactly, detailed models differ in their closure approaches. Two classes of detailed models include variants of the method of moments (MOM) and the sectional methods.

Popular MOM variants include the method of moments with interpolative closure (MOMIC) [25], the quadrature methods such as the direct quadrature methods of moments (DQMOM) [26] and the conditional quadrature methods of moments (CQMOM) [27], and the hybrid method of moments (HMOM) [28] which blends DQMOM and MOMIC concepts for a numerically robust method that captures the bimodal nature of the NDF. When applied to the model DLR aero combustor case [29], however, both HMOM and CQMOM differ in their predictions between the models and with the experimental soot volume fraction (SVF) data. In the sectional method approach, the PSDF is modeled using a discrete number of sections based on a particle property, such as volume [30]. The sectional method has been applied to both laminar [31] and turbulent flames [15, 32] with good accuracy relative to the experimental data but can be very computationally expensive depending on the number of sections used. Numerical studies with a sectional model [15] suggested that the evolution of the PSDF from unimodal to bimodal is due to a time-history effect of the soot chemistry along the flame. Recently, a bivariate multi-moment sectional method (BMMSM) [16] was developed by blending the sectional approach with HMOM resolving both the NDF and PSDF. BMMSM was compared against experimental data for a laminar premixed flame and a turbulent jet flame. For both cases, the BMMSM approach was in good agreement with the measured SVF, including capturing the bimodal PSDF of the turbulent case [16]. Other numerical studies using HMOM [29, 33], CQMOM [29], and BMMSM [16, 34] highlight the importance of modeling the intermittent and time dependent behavior of soot.

The above outlines that there is a time-history effect that is difficult to capture even with the most advanced soot models available. This highlights that there remains a need to understand the time-history dependence on soot formation, to identify key conditions promoting soot formation, and to develop an approach to identifity difficiencies in a soot model relative to experimental data. Furthermore, due to the intermittent nature of soot formation, long simulation times with multiple flow through times are required. This creates the need for an engineering soot model and novel approach that can be applied to a variety of cases. In order to understand the time-history effect of soot formation and evolution, we propose a statistical approach to identify the key variables (*i.e.,* temperature, fuel-air-ratio, chemical species, mixture fraction, *etc.)* leading to soot formation. In our recent study [35] on the model DLR aero-combustor, a two-equation semi-empirical soot model achieved good agreement with the experimental SVF data and other computational studies.

To collect time-history statistics, we inject massless tracer particles near the dome-face region of the combustor. These particles store the time history evolution of the solution variables. We then define an area of interest (AoI) based on combinations and ranges of each of the solution variables, which are then analyzed over the entire particle trajectory. The time-history correlation results for each variable are then compared to the experimental SVF data to determine which of the time-history effects best correlate to soot formation. A similar particle tracking approach was taken by Chong et al. for the DLR combustor. However, we expand our analysis based upon the defined AoI and time-history based correlations to the experimental data [33, 36].

NUMERICAL SETUP

In this study, we used the OpenNCC code (the releasable version of the National Combustion Code), which has been continuously updated for more than two decades at NASA Glenn Research Center. To resolve unsteady turbulent and complex swirling motions seen in the DLR combustor, Large Eddy Simulation (LES) with a non-linear k-epsilon turbulence model [37] was used. In this paper, we present CFD results for the 'primary air only' (*i.e.,* no side jets) experimental configuration, based on the operating conditions summarized in Table 1.

In the following subsections, brief descriptions of the flamelet progress variable approach, two-equation soot model, and particle-based statistical approach are provided.

TABLE 1: OPERATING CONDITIONS FOR DLR COMBUSTOR AT P = 3bar

	Ring air	**Central air**	**Fuel** (C_2H_4)
Mass flow rate, g/s	7.08	3.03	0.83
Temperature, K	297	297	293

Multiple Time-Scale Flamelet Progress Variable Method (MTS-FPV) and Chemical Kinetics Mechanism

A recently implemented and validated Multiple Time-Scale Flamelet Progress Variable Method (MTS-FPV) [38, 39] was used for soot-modeling. The key feature of the MTS-FPV approach is to solve the transport equations for the mean mixture fraction ($\overline{Z}$), its variance (*Vz*), and mean progress variable ($\overline{Y}_p$), which have a relatively shorter time-scale.

The computation of the relatively longer time-scale quantities like soot uses a secondary progress variable approach where additional progress variables, $\overline{Y}_{p,j}$, are solved for each soot variable [40] as follows:

$$\frac{\partial}{\partial t}\left(\overline{\rho}\,\overline{Y}_{p,j}\right)+\frac{\partial}{\partial x_i}\left(\overline{\rho}u_i\overline{Y}_{p,j}\right)-\frac{\partial}{\partial x_i}\left(\overline{\rho}(D+D_T)\frac{\partial\overline{Y}_{p,j}}{\partial x_i}\right)=\overline{\dot{S}_{p,j}}$$

In this work, two additional secondary progress variables ($\overline{Y}_{p,C(s)}, \overline{Y}_{p,N}$) are solved for the soot mass-fraction, *C(s),* and soot number-density, *N*. The source terms $\overline{\dot{S}_{p,j}}$ for the progress variable equations are provided by a semi-empirical two-equation soot model developed by Fairweather *et al [24].* The simplified soot nucleation and growth mechanism proposed by Leung *et al.* [40] was used, which assumes that acetylene is the only soot nucleation and surface growth species. The soot oxidation source term is modeled by including the contributions of O_2 and *OH* species, following the work of Liu [41] and Kennedy [42]. In summary,

$$\overline{\dot{S}_{p,j}} = S_1 + S_2 + S_3$$

where S_1, S_2, and S_3 are the soot nucleation, surface-growth and oxidation source terms, respectively [24].

The current approach does not include any contributions of soot mass-fraction in the flamelet table, which can be a source of error in the soot predictions. Further details of the MTS-FPV approach for OpenNCC are provided in [35].

The choice of the chemical kinetics mechanism can play a critical role in soot predictions, and was reported by Franzelli *et al.* [43]. In the current study, a 75 species mechanism developed by Wang *et al.* [44] was used. This mechanism includes mono-aromatic species of benzene and its derivatives. The C_2 and C_3 chemistry for ethylene was described by a series of steps that convert C_2H_4 to C_2H_3 and C_2H_2.

Some key features and inherent limitations of the current implementation of the acetylene-based semi-empircal model are summarized as follows:

1. This model uses only acetylene as the soot precursor and ignores the PAH species and other gaseous soot precursors (*e.g.,* benzene, pyrene, etc.). This assumption simplifies the soot nucleation process which is influenced by temperature and the PAH species concentration, especially in regions of very rich mixture fractions (see [43, 45].)
2. Some degree of turbulence-chemistry-soot interactions (TCSIs) is indirectly taken into account by solving for the variance of mean mass fraction, *Vz,* and sub-filter turbulent kinetic energy (TKE). However, the sub-filter scale TCSIs are not explicitly modeled in the current work. In previous work for the DLR combustor, Chong, *et al. [33]*]) have reported that acetylene (C_2H_2) concentrations are not significantly influenced by small-scale dissipation rate fluctuations.
3. The soot formation and evolution is known to occur by a very specific range of gas-phase compositions [46]. However, the current model utilizes the smooth functions of C_2H_2, *OH* and O_2 for all soot formation and oxidation mechanisms, and thus, any sharp local variations in species concentration that favor soot-formation cannot be explicitly resolved.
4. The soot oxidation processes are surface reactions with hydroxyl radicals *OH* and O_2, and these processes are fundamentally different process [45]. The oxidation model implemented in this simple soot model might not be able to distinguish between the two events.
5. Time scales of nucleation and surface growth are relatively long, compared with the faster time-scales of oxidation. It is questionable whether the current semi-empirical model can adequately address the disparate time scales of soot formation and oxidation.

One of our primary objectives in this study is to address some of the weaknesses of the semi-empirical soot model by proposing modifications based on time-history correlation data, and improve soot prediction accuracy based on a novel particle-based statistical approach.

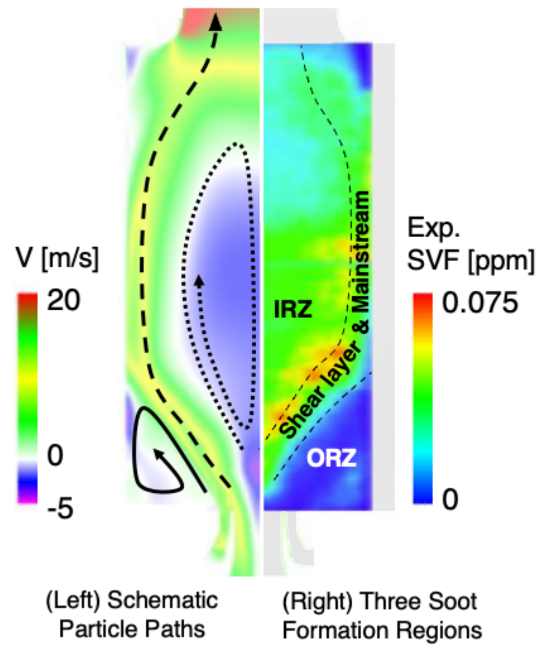

FIGURE 2: SCHEMATIC PARTICLE PATHS AND THREE DIFFERENT SOOT FORMATION REGION OVERLAYED ON THE EXPERIMENTAL SOOT MEASUREMENT [1]

Novel Particle-based Statistical Approach

This subsection provides a detailed description of the proposed particle-based statistical approach that attempts to include the time-history of flow quantities and species in order to improve the soot predictions of the 'baseline' two-equation semi-empirical model of Fairweather *et al.*[24].

In the DLR combustor, as shown in the time-averaged axial velocity contour from our previous study [35] and the experimental soot measurement [1] there are three primary flow regions: outer recirculation zone (ORZ), inner recirculation zone (IRZ) and the shear layer/mainstream region (See Fig.2). Primary areas of soot formation are the shear layer/mainstream region and IRZ. As reported by the DLR team [8], the soot formation takes place in the pockets of rich burned gas occasionally generated through the interactions between a precessing vortex core (PVC) in the inner shear layer and double helical vortex in the outer shear layer. Soot quickly oxidizes in the *OH*-rich lean burned gas regions. The net result is that there is a high soot volume fraction measured in the inner shear layer and mainstream region (and partially IRZ) originating from the exit of the air/fuel injector. In addition, very low SVF is observed in the ORZ regions.

In order to further understand the unique and complex mechanisms of soot formation in the DLR combustor, we injected 10,000 massless particles downstream of the injection region randomly in space and time while solving unsteady flow field within the computational domain. The shape of the particle injection area is an annulus located at the axial location, Δx_{inj} = 0.01m and radial width ΔR_{inj}, (see Fig. 1). The injected particles

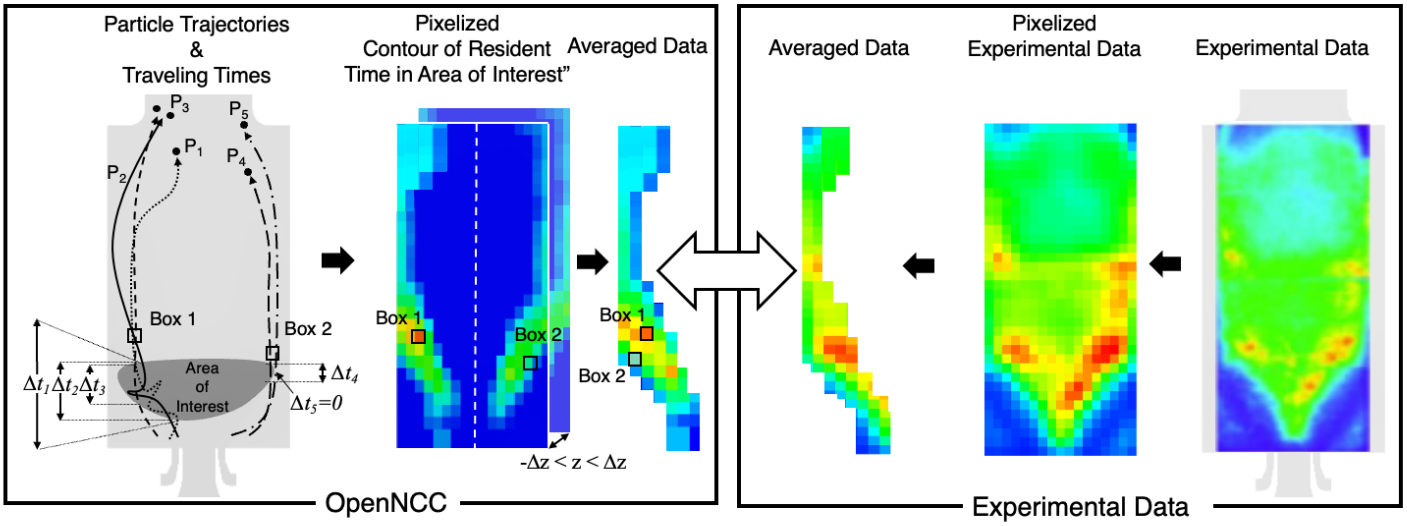

FIGURE 3: SCHEMATIC OF PARTICLE BASED STATISTICAL APPROACH

mainly travel downstream along the shear layer, and time-history information at each CFD time-step is collected for multiple local variables (*T, P, ρ, u, v, w, TKE,* $\overline{Z}$, *Vz, XI,* $\overline{Y}_p$, source terms of soot models, and species, Y_i).

A similar particle tracking analysis was performed by Chong *et al.* [33, 36], who also utilized a Lagrangian approach to calculate 1,000 particle-like trajectories during an LES calculation. Based on primary trajectories, the particles were categorized into three types: Type 1 (along the shear layer/mainstream region), Type 2 (inside ORZ) and Type 3 (inside IRZ). Based on their analysis of the different intermittent frequencies of soot generation, Type 1 particles experienced high soot production, compared with Type 2 and Type 3. It was also reported that Type 1 particles have the highest percentage of particle types in the combustor, regardless of the operating conditions. Based on their observations, only Type 1 particles were chosen in this study, in order to obtain better statistical convergence of particle data for soot model improvements. Representative trajectories of some of the 10,000 Type 1 particles in the current work are shown in Fig. 3 (P_1, P_2, P_3, *etc.*).

The time-history based statistical approach for proposed soot-modeling improvement consists of seven steps as schematically described in Fig. 3:

Step 1: First, the area of interest (AoI) (based on a specific ranges and combinations of temperature, equivalence ratio (ϕ), species concentration, [C_2H_2], *etc.*) is defined.

Step 2: The massless particles (P_1, P_2, P_3, P_4,, P_5, ... $P_{10,000}$) are randomly injected within the upstream region (the gray region in Fig. 1). Each particle's trajectory is determined by the local velocity field at each time-step of the computation. The residence time of each particle in the AoI is recorded (Δt_1, Δt_2,.... $\Delta t_{10,000}$). If a particle does not reach the AoI, the residence time is set to zero (see P_5 in Fig.3, Δt_5=0).

Step 3: Post-processing: At the end of particle data collection, lasting approximately one flow through time-step, particle statistics within spatial bins or boxes (denoted by Box 1, Box 2, …) are calculated. The location and size of the boxes are defined such that enough tracer particles are captured while preserving important features of the experimental data. For our application, a box size of 3x3mm meets this criteria. The length of the box in the normal direction of the plot is -Δz < z < Δz. The particle-based averaged residence time (τ) of each Box based on the AoI is calculated by ensemble average of Δt of all particles reaching the box. (For example, $\tau_{Box,1}$ = (Δt_1+Δt_2+Δt_3)/3 and $\tau_{Box,2}$ = (Δt_4+Δt_5)/2 in Fig. 3).

Step 4: The pixelized contour plots of residence time (τ) are constructed.

Step 5: Finally, the contour is folded along the white-dashed line (*i.e.*, centerline) for averaging (See Fig. 3), and all pixels where the number of particles reaching the box is less than the threshold, N_t, are ignored. In the current work, N_t = 10 was chosen after a sensitivity study of the effect of N_t on correlation amongst variables deemed to be of primary influence on soot predictions.

Step 6: Similar to **Step 5**, the experimental profile of the soot volume fraction is pixelized and folded for averaging.

Step 7: The correlation coefficient, which refers to "time-history correlation coefficient" (THCC), between the two pixelized profiles (CFD particle data and experimental data) is calculated.

A key physical interperation of the THCC is to identify the time-history that the fluid (*i.e.,* massless tracer particles) experiences before it reaches the AoI location, and what happens to a particle after it passes throuth the AoI. In this study, we choose the residence time of fluid staying in the AoI, where the AoI is defined by combinations of ranges of temperature, local equivalence ratio, chemical species, etc. We then construct the contour map of the residence time for all particles identified by the AoI. We finally calculate the THCC with respect to the contour map of the experimental measurement of soot volume-fraction (SVF) in regions where the AoI particles exist (See. Fig. 3). A strong correlations means that the time-history of the

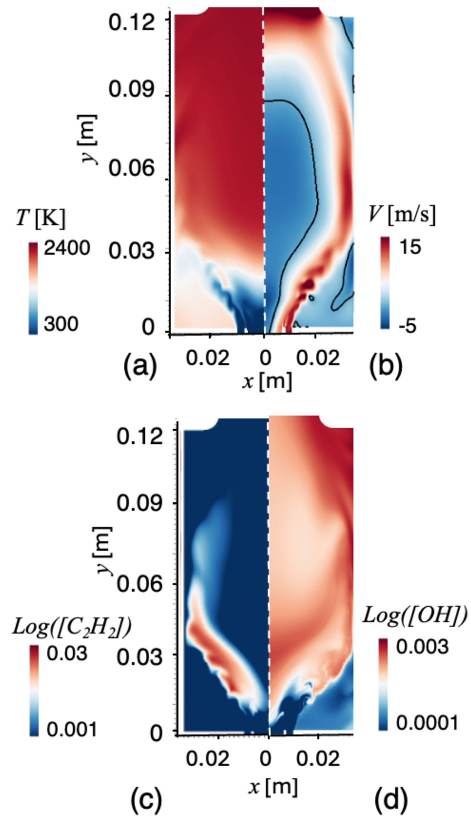

FIGURE 4: CONTOURS OF INSTANTANEOUS FLOW FIELDS, (a) TEMPERATURE, (b) AXIAL VELOCITY, (c) LOG([C_2H_2]), and (d) LOG([OH])

defined AoI is important for soot formation of the studied case. This analysis can thus provide insight into a question like: "if a reactive pocket of gas stays in a fuel rich region for a long time at a specific temperature, then how does such a time-history of the fluid in that region produce soot at a later time or location?"

In summary, the calculated THCC is a fundamental quantity in the context of the present work. It quantifies the importance of history-based soot formation of the gas, which experiences a specific range of species composition, thermochemical state, as well as flow fields (including strain rate, turbulence, *etc*.), with its residence time within the AoI. More importantly, the outcome of this analysis could suggest the locations where the soot model fails to accurately capture underlying physics of soot formation. To the best of the authors' knowledge, this type of analysis has not been reported in the literature in the context of being used to improve semi-empirical soot model predictions for engineering applications.

A total of 1000 Ivy-Bridge processors on Pleiades at the NASA Advanced Supercomputing facility were used to perform the LES calculations. The overall computational time was approximately 240 wall clock hours per flow-through cycle of 20 [m-s]. For the LES, all the time averaged data shown in the following subsections were obtained over the final two flow-through times of computation [35]. The 10,000 massless particles were randomly injected into the domain over the final ~16 [ms] of the LES computation. The calculations were performed on an unstructured mesh with 12.2 million elements (2.5 million nodes) and is identical to that used in the work of Chong *et al.* [33] which had already undergone a mesh refinement study.

RESULTS AND DISCUSSION

Calculated Flow Fields and Validation

The instantaneous flow fields (temperature, axial velocity, concentrations of C_2H_2 and *OH*) are depicted in Figs. 4 (a) – (d). In the temperature field, the fuel rich shear layer originates from the fuel port and ignites around $y = 0.03$ [m] after mixing with the hot product. Along the center line ($x = 0$ [m]), cold lean region exists up to 0.01 [m], and then, one of the key soot precursors, C_2H_2, starts forming while temperature is gradually increasing (See Fig.4 (b)). This region is associated with the tip of the upper inner recirculation zone (IRZ). It is reported by Litvinov *et al.* [8] that intermittent and unsteady flow fields are generated through the interactions between the PVC and the double helical vortex. This is the most critical region for the soot formation in this combustor. The *OH*-rich lean-burn gas region is located slightly downstream, where the soot quickly oxidizes. The unique feature of the V-shape soot formation observed in the experimental data (See Fig. 2 [1] and Fig. 4 (c)) coincides well with the C_2H_2 contours, implying that C_2H_2 is indeed important for the soot formation. It is well-known that the higher carbon species (e.g., the PAH species) are also rich in the region and play a critical role as soot precursors [47-49].

It is crucial to get a realistic CFD flow field before performing the particle-based statistical approach. To check the validity of the calculated flow field, the time-averaged axial and radial velocity components at three different axial locations (y=7 [mm], 26 [mm] and 46 [mm]) were compared with the experimental measurements [1] (see Figs.5 (a)). As reported in Ajmani *et al., [35],* the agreement between the measurements and the CFD predictions is satisfactory. However, the predicted soot volume fraction using the empirical soot model (see Fig.5 (b)) shows noticeable discrepancy, especially in the upstream region, the near-wall regions downstream, as well as in the center recirculation region. The modeling uncertainty can thus use considerable improvement, with the possible inclusion of time-history effects proposed in our current work.

Before investigating the results from the particle-based statistical approach, it is necessary to confirm that a sufficient number of particles are being used for obtaining statistically converged statistics. Figure 6 (a) shows a contour of the variation in the number of particles which reach each box over the 16ms duration of particle injection. The box size is set to be 3 [mm] to pixelate the domain, and the length of the box in the normal direction of the plot, Δz, is 5 [mm]. The dashed line indicates the optical view region in the experiment [1]. Figure 6 (b) shows the averaged profile inside the optical view after folding two sides

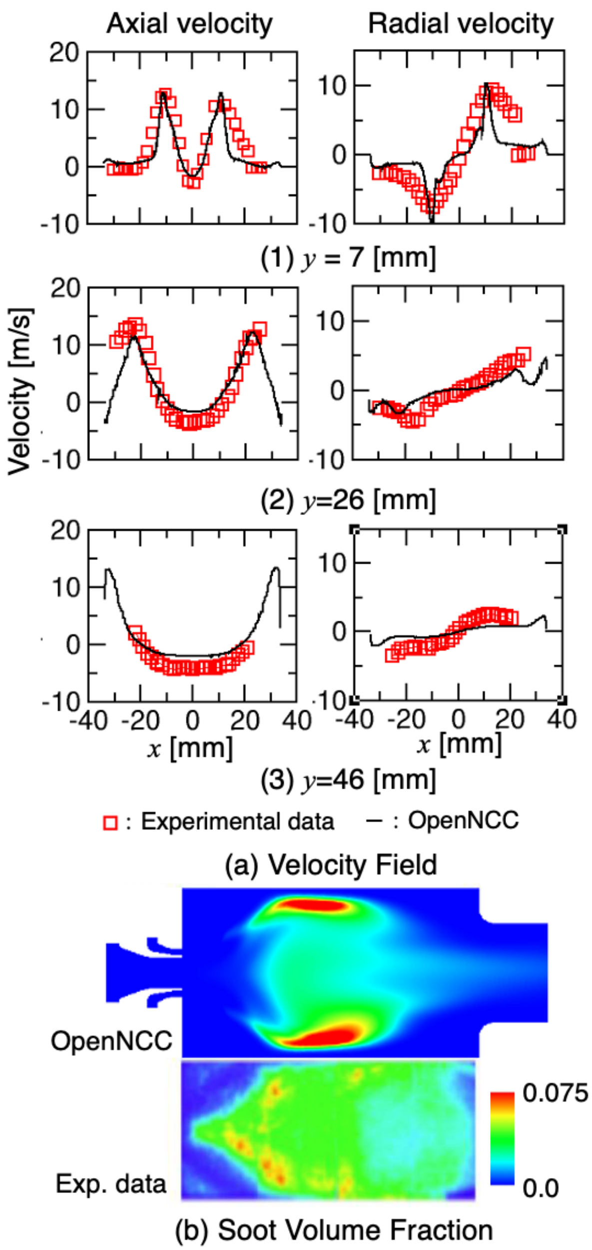

FIGURE 5: (a) TIME-AVERAGED AXIAL AND RADIAL VELOCITY and SOOT VOLUME FRACTION PROFILES AT DIFFERENT AXIAL LOCATIONS: (1) Y=7 [MM], (2) Y=26 [MM], AND (3) Y=46 [MM] COMPARED WITH THE EXPERIMENTAL DATA [1]

into one side across the centerline (see **Step 5** in the previous section). We performed the sensitivity analysis of N_t against the statistics and decided to use $N_t = 10$.

Figures 7(a) and (b) show the time-averaged temperature and equivalence ratio (ϕ) contours from the LES calculation [35], compared with the current particle-based averaging process. Particle-based averaged temperature and equivalence ratio of the i^{th} box are calculated by: $\bar{T}(i) = \sum_n \int_{t1}^{t2} T(t)dt \,/\, \sum_n \int_{t1}^{t2} dt$ and $\bar{\phi}(i) = \sum_n \int_{t1}^{t2} \phi(t)\, dt \,/\, \sum_n \int_{t1}^{t2} dt$, where, n is the number of particles reaching the i^{th} box, and t_1 and t_2 are physical times when a particle enters and

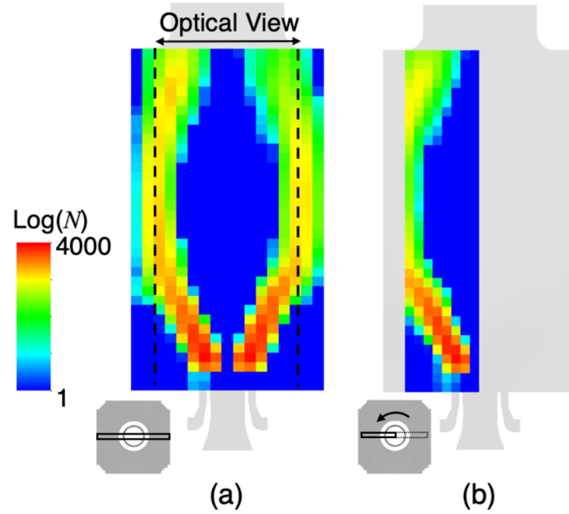

FIGURE 6: CONTOURS OF TOTAL NUMBER OF PARTICLES USED FOR THCC ANALYSIS (a) FULL DOMAIN AND (b) TWO-SIDE AVERAGED PROFILE

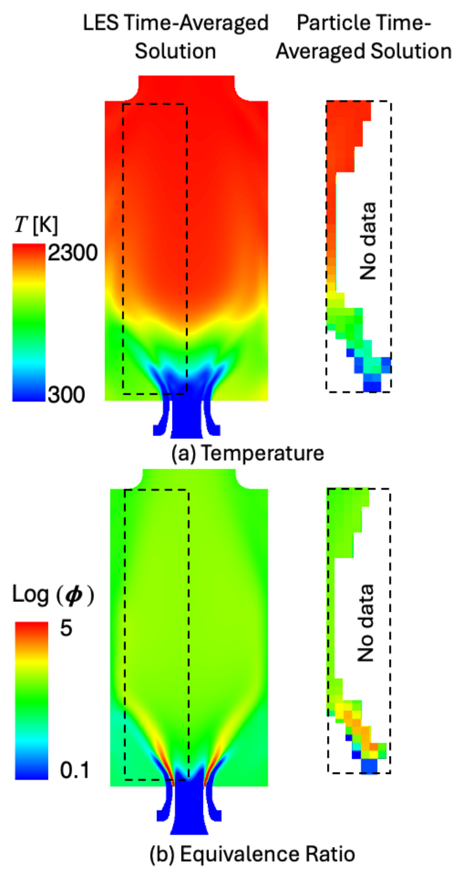

FIGURE 7: LES TIME-AVERAGED SOLUTION OF (a) TEMPERATURE AND (b) EQUIVALENCE RATIO FROM LES (left) AND (right) PARTICLE TIME-AVERAGED SOLUTION

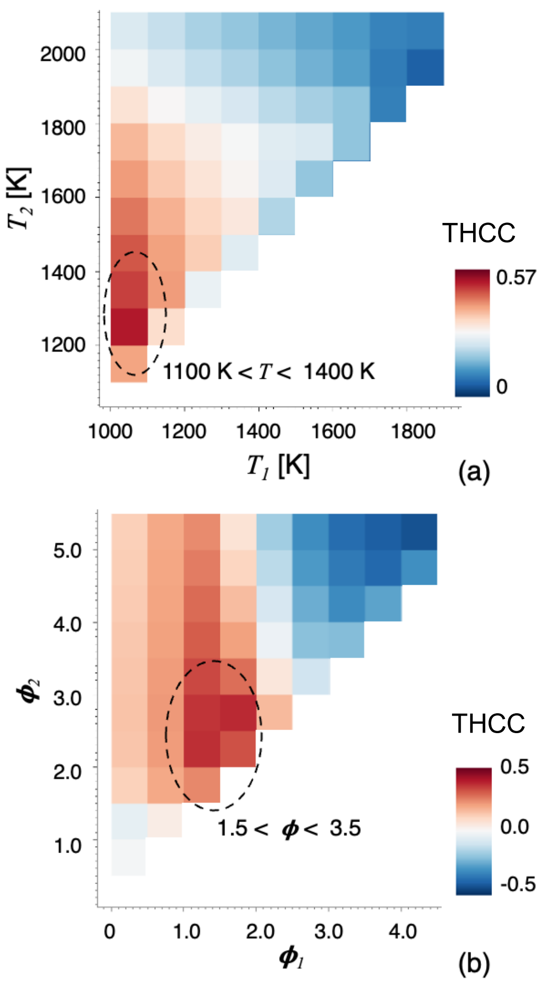

FIGURE 8: THCC MATRICES OF (a) TEMPERATURE AND (b) EQUIVALENCE RATIO

leaves the box, respectively. With a sufficiently large number of particles, n, the particle-based averaging process should give the same answer as the one from the time-averaged LES result (as seen in Figs. 7). The blank regions in the right column of Figs.7(a) and (b) are the areas where n is less than N_t, and the particle history data in this region is deemed statistically insignificant and thus omitted for the statistical based analysis below. As discussed in the previous section, only 'Type 1' particles (which would consist of > 75% of the total number of particles if the injection was spread across the entire cross-sectional area of the fuel inlet), as categorized by Chong *et al.* [33] are considered in this study.

Effect of Temperature and Equivalence Ratio

In this subsection, the critical regions of temperature and equivalence ratio are investigated, as based on the THCC correlation with respect to the experimental measurement of SVF [1]. To make the correlation matrix as in Fig. 8 (a), the temperature range (*e.g.,* 1000 [K] < T < 2100 [K]) is first divided into ten regions in intervals of 100 [K]. The residence time of

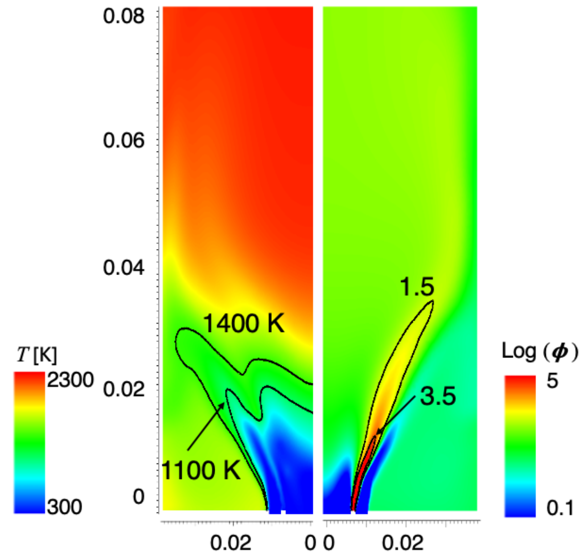

FIGURE 9: TIME-AVERAGED TEMPERATURE AND EQUIVALENCE RATIO PROFILES WITH CONTOUR LINES

particles in each temperature region (T_2 < T < T_1) is then calculated as in Steps 2-3. The THCC for each range is summed up in Fig. 8 (a).

First, it is observed that there is a noticeable trend that the region where particles reside in a specific temperature region (*e.g.,* 1100 [K] < T < 1400 [K]) for a relatively long time, has a higher THCC with the experimental measurement of the SVF. On the other hand, the opposite trend is seen for the high temperature region of T > 1800 [K]. The maximum THCC is 0.57, implying that the effect of time-history of temperature is statistically important with respect to experimental SVF. A similar analysis is done for the equivalence ratio, ϕ, and the resulting correlation matrix is shown in Fig. 8(b). It is also found that there is a soot (un)favorable region of ϕ *(1.5 <* ϕ *< 3.5)* in terms of the time-history effect. Although there are many other parameters (hyper-parameters) involved in the soot formation, it is necessary to interpolate these results with care. These observations are consistent with the "soot bell curve" or "soot island" formation threshold, where the soot concentration peaks within a specific range of conditions [50]. Furthermore, it is well known that the soot formation is favored in a fuel-rich region and the soot oxidizes in the hot region in the presence of hydroxyl radical, OH, molecular oxygen O_2, and atomic O [51]. These specific regions are overlayed on the time-averaged LES results of temperature (left) and equivalence ratio (right) in Fig.9.

Next, the AoI is further investigated by the combination of the two specific ranges of temperature and equivalence ratio, and the resulting THCC matrix with respect to the experimental SVF is shown in Fig. 10. Although these two quantities are strongly correlated to each other, the non-uniformity of the THCC map seems to imply that there are different regions with differing mechanisms controlling soot formation in the different areas of the combustor. We identify three distinct regions showing relatively large value of T *vs* ϕ correlation: **Region (1)** 1000 [K] < T < 1300 [K] and 0.5 < ϕ < 2.5, **Region (2)** 1000 [K]

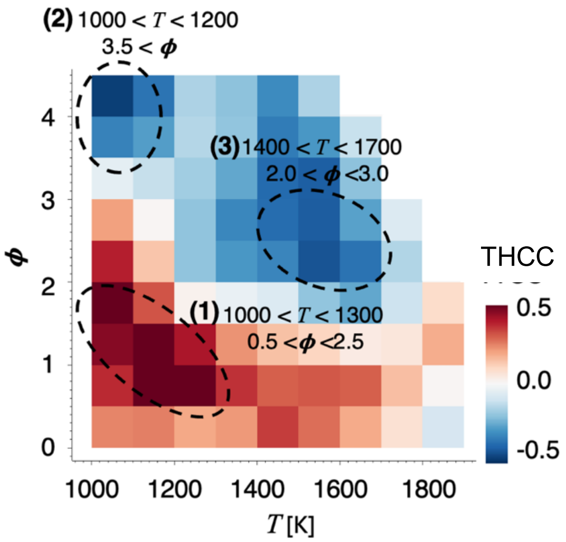

FIGURE 10: THCC MATRICES OF TEMPERATURE AND EQUIVALENCE RATIO

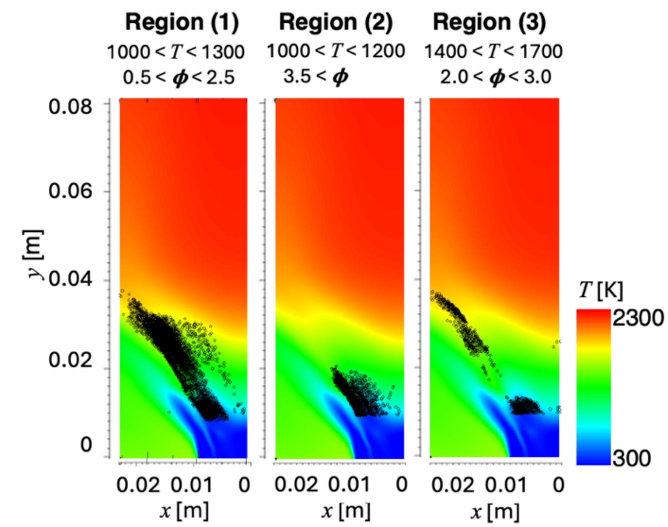

FIGURE 11: TIME-AVERAGED TEMPERATURE WITH SPECIFIC RANGE OF TEMPERATURE AND EQUIVALENCE RATIO (dark dots)

< T < 1200 [K] and 3.5 < ϕ, and **Region (3)** 1400 [K] < T < 1700 [K] and 2.5 < ϕ < 3.0. The corresponding regions overlayed on the time-averaged LES temperature contours are shown in Fig. 11 (the black dots are the particle locations in the AoI). **Region (1)** corresponds to the inner side of the shear layer, the moderately fuel-rich region where the fuel and oxidizer rapidly mix together. Experimental [8] and numerical [33] studies have reported the importance of this region for soot formation. **Region (2)** is the very fuel-rich cold region, which is near the upper tip of the IRZ. Finally, **Region (3)** seems to be a combination of **Region (1)** and **Region (2)**. It is worth mentioning that all three regions include the upper tip of the IRZ. Litvinov, *et al.* [8] experimentally observed that this location is full of intermittent mixing of pockets of rich burned gas, *OH*-rich lean burned and cold air. Multiple numerical results have also reported this intermittent behavior (*e.g.,* [33, 45]). It is important to draw the conclusion that the time-history (longer or shorter) of gas pockets staying within these specific regions are indeed strongly correlated with soot formation. In other words, any soot model which does not include this kind of time-history effect, could miss some critical physics of the soot formation.

Investigation of Critical Species

In this study, the 75 species mechanism for ethylene combustion, developed by Wang *et al.* [44] was used. For the statistical analysis, it was necessary to identify the key species which play an important role in soot formation, particularly in the context of their time-history effect on nucleation, surface growth and oxidation of soot. As a first step, twenty five species were identified, based on having a good match between CFD species trends and experimental SVF. Each species was then used as a co-variable to study how it would impact the partial correlation between the CFD and experimental SVF. Only the species that met the criteria of "p-value < 0.005 for 95% confidence interval" were retained, and the rest were rejected.

TABLE 2: LIST OF SELECTED SPECIES AND CORRELATIONS

Species	Max concentration	CC with Exp. Data (soot)	Max. THCC. with Exp. Data (soot)
O	2.10E-04	0.07	0.45
O_2	1.60E-01	-0.17	0.73
H_2	4.00E-03	0.018	0.43
OH	2.00E-03	0.17	0.65
CO	7.30E-02	0.37	0.21
HCO	1.60E-06	-0.4	0.74
CH_2*	1.20E-07	-0.24	0.76
C_2H_2	2.70E-02	-0.27	0.73
C_2H_4	2.60E-01	-0.48	0.75
C_3H_3	2.40E-05	0.08	0.57
C_4H	6.00E-08	-0.15	0.45
C_5H_5	2.80E-06	0.2	0.4
C_6H_5	5.60E-07	0.19	0.63
C_6H_6	2.20E-04	-0.15	0.36

: Max. Corr. Coeff. Time-His. with Exp. Data > 0.6

The selected fourteen species, and their respective molar concentrations, correlation with respect to experimental SVF, and time-history correlations (THCC) are listed in Table 2. A brief description of the species selection criteria is provided below:

1. Fuel and small hydrocarbons (C_2H_2, C_2H_4, C_3H_3)
2. Oxidation species (OH, O, O_2, H_2). Although H_2 is not a direct oxidant, it was evaluated because it is a by-product indicating a spontaneous process relevant to soot formation has occurred [52]. In order words, as aromatic species are formed and large complex PAH species appear, their growth leads to an overall reduction of the Gibbs free energy via H_2 release [52].

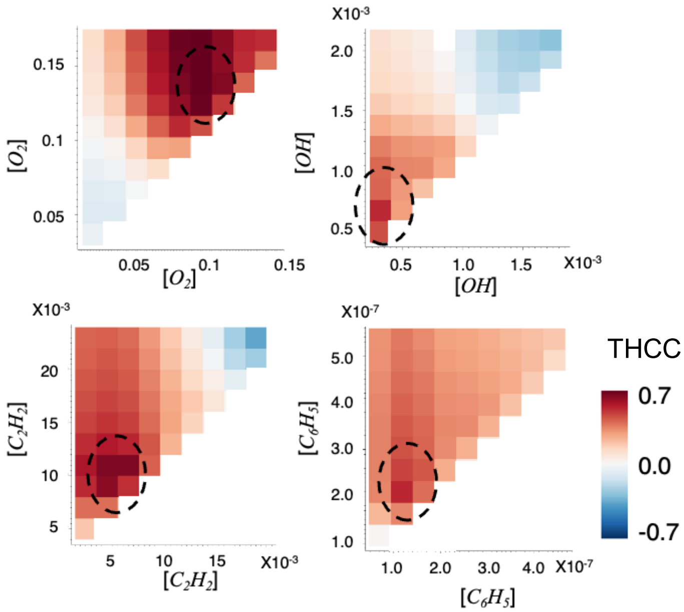

FIGURE 12: THCC MATRICES OF [O_2], [OH], [C_2H2] AND [C_6H_5]

3. Species that can be measured (*CH*, etc., CH2** was initially selected as a *CH** representative)
4. Aromatic Species (*C_6H_6, C_6H_5*). Benzene, *C_6H_6*,[44, 53] and phenyl ,*C_6H_5*, [54-56] were evaluated as they both are key species involved in the formation of higher order aromatic compounds which influence soot nucleation.

To further reduce the number of species, two types of correlation coefficients (CC) were used. The first CC is computed using the particle-based averaged profile of each species with respect to the experimental measurement of soot (third column of Table 2). The second is the THCC of the species with the experimental soot measurement (fourth column of Table 2). It is interesting to observe that many species such as *O_2, OH, and C_6H_5*, show very strong THCC, which is why they are selected, even though they show very weak CC with respect to experimental data. The trend is reversed for some species (*e.g.*, *CO*), which is cause for them to be eliminated. These trends seem to indicate that different species have a different way to contribute to soot formation, particularly when their time-history effect is included in the correlation calculations.

The calculated THCC matrices with respect to experimental SVF for some selected species (*O_2, OH, C_2H_2, and C_6H_5*) are shown in Fig. 12. The region inside the dashed circle indicates the range of species concentration where the time-history effect is tightly correlated with the soot formation. The corresponding regions from the LES time-averaged solution are shown in Fig. 13. There are two iso-contour lines corresponding to the region inside the black dashed circles in Fig.12. For instance, the residence time of particles inside the AoI (0.005 < [C_2H_2] < 0.0125) shows a strong correlation with the soot measurements with statistical significance. For [O_2], there is a strong correlation between the residence time inside the AoI (0.1

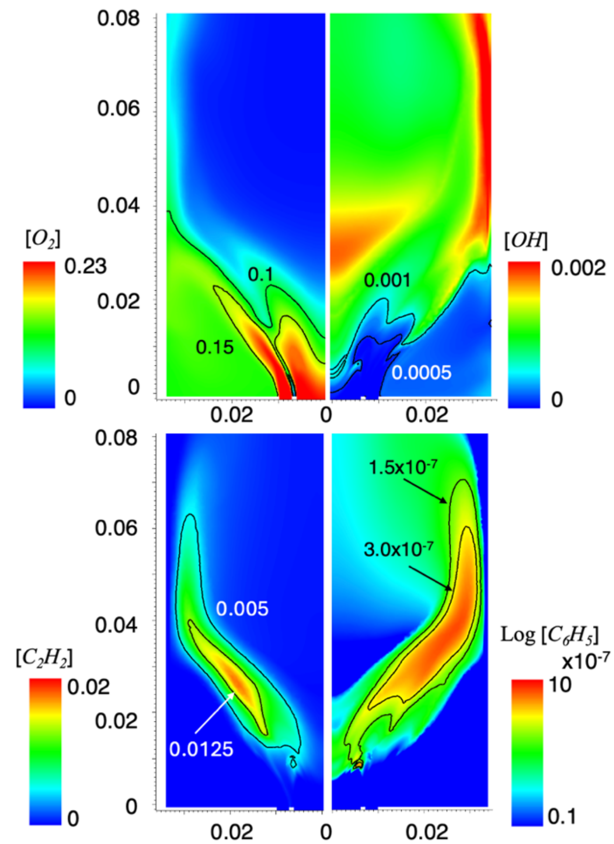

FIGURE 13: LES TIME-AVERAGED SPECIES PROFILES WITH CONTOUR LINES

< [O_2] < 0.15) and the soot profile, which corresponds to the location where the cold air starts mixing with hot-products and the oxidization of the soot begins to takes place.

Utilizing the THCC with the experimental measurement of soot enables us to down-select critical species (*i.e.*, *O_2, OH, HCO, CH_2*, C_2H_2, C_2H_4,* and *C_6H_5*) that could be used to improve the soot model by considering the time-history effect (please note that *C_6H_6* is not selected due to the low THCC although it is known to a precursor species for PAH formation).

All seven species show a statistically significant result that their time-history effect on the soot formation is important. For the purpose of improving the current two-equation soot model, it is still necessary to eliminate some additional species which are strongly correlated to each other, and hence do not provide the necessary orthogonality for model improvement. For example, *HCO*, which is a good marker of the heat release [57], is strongly correlated with the temperature. *CH_2** and *C_2H_4* are also strongly correlated with the *C_2H_2* and *ϕ*, respectively. Finally, considering the structure of the soot model and the relatively strong correlations of *HCO (CC=-0.8), CH_2** (CC=-0.88), and *C_2H_4 (CC=-0.74)* with respect to *OH*, these three species were eliminated. For the completeness of analysis, the correlation matrix for selected quantities is provided in Appendix.

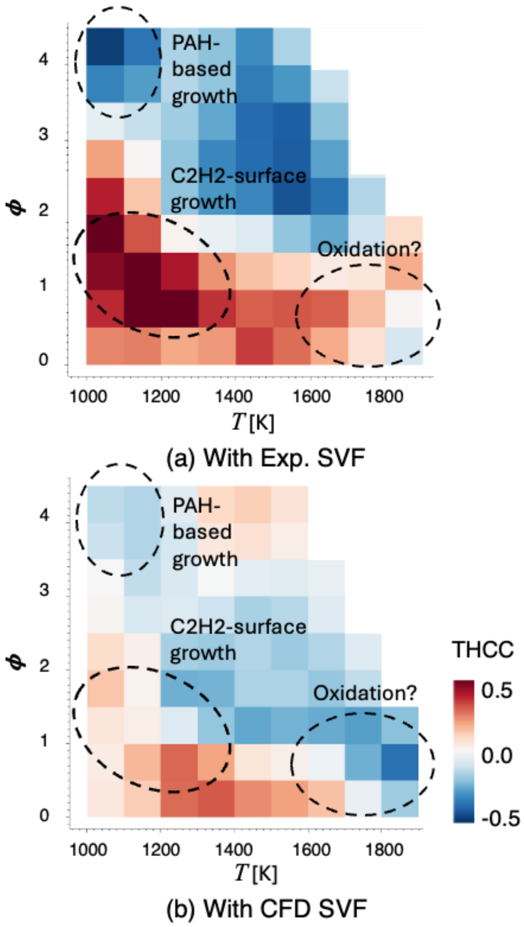

FIGURE 14: THCC MATRICES OF TEMPERATURE AND EQUIVALENCE RATIO USING (a) EXPERIMENTAL SVF AND (b) SVF CALCULATED BY THE SOOT MODEL

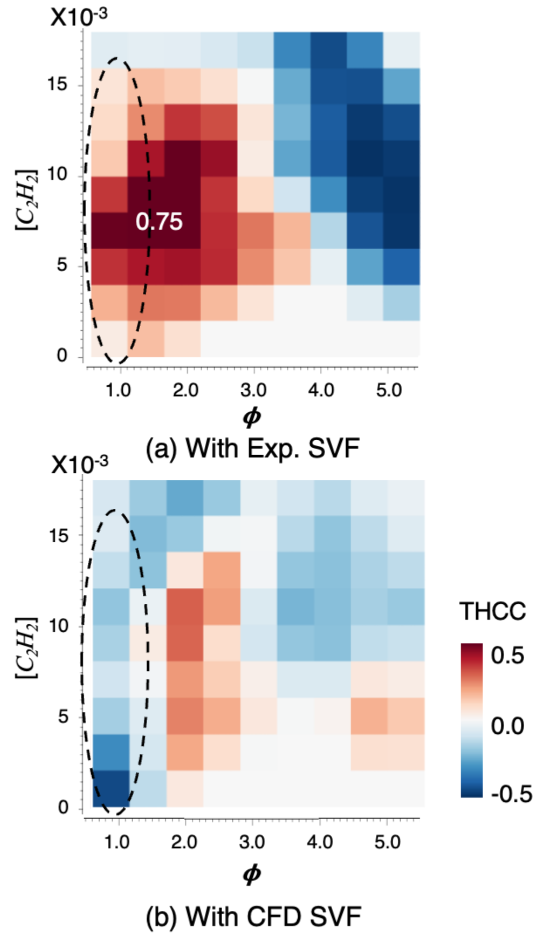

FIGURE 15: THCC MATRICES OF [C_2H_2] AND EQUIVALENCE RATIO USING (a) EXPERIMENTAL SVF AND (b) SVF CALCULATED BY THE SOOT MODEL

It is perhaps significant that after using large amounts of particle history data, a down-selection process based on the THCC with respect to experimental SVF indeed leads us to select the species (*e.g.*, O_2, OH, C_2H_2, and C_6H_5), which are known to be the major influencers in semi-empirical modeling of soot formation for the DLR combustor studied in this work.

Model Inadequacy and Modifications

In this subsection, we would like to develop further discussion about how to utilize the THCC results in terms of possible improvements made for the current empirical two-equation soot model. So far, the THCC results reveal that the time-history effect on the soot formation is statistically significant for some quantities such as temperature, equivalence ratio, and concentrations of certain species (*i.e.*, O_2, OH, C_2H_2, and C_6H_5). However, these observations need to be coupled with the physical understanding of soot formation mechanism so that the findings are properly incorporated in the possible modifications for the soot model.

As the first step to propose the soot model improvement using the time-history effect, we would like to revisit the result of the THCC matrix between T and ϕ with the experimental data (see Fig. 10) in order to verify how accurately the current model can capture the THCC for a specific range of parameters. To this aim, the THCC matrix between T and ϕ with the SVF predicted by the current soot model is calculated (see Fig. 14 (b)). The comparison between Fig. 14 (a) and Fig. 14 (b) tells us about the region(s) of the parameter space where the current soot model (in)accurately takes into account the time-history effect. There are three different regions showing noticeably different THCC between the two plots. The physical interpolation of each region and possible modifications for the soot model are provided below.

Region 1: 1000 [K] < T < 1300 [K] and 0.5 < ϕ < 2.0

In this region, the THCC with the experimental data shows very strong correlation (*i.e.*, the time-history effect is statistically significant), however, the model does not capture such a trend accurately. The authors speculate that this moderately rich mixture fractions region is mainly related to the acetylene-based surface growth [33] and suggest that S_2 in Eqn .(1) needs to be improved. Selecting the variables of a function

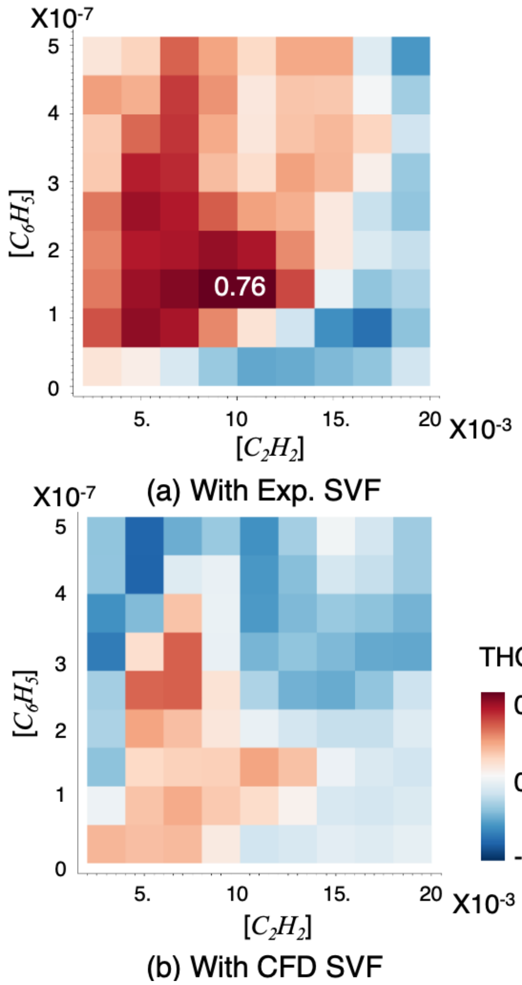

FIGURE 16: THCC MATRICES OF [C_6H_5] AND [C_2H_2] USING (a) EXPERIMENTAL SVF AND (b) SVF CALCULATED BY THE SOOT MODEL

to improve the S_2 term is a non-trivial task. Based on the current soot model and the previously selected quantities, it might be natural to choose the following two functions: S_2*([C_2H_2], T, τ) or S_2*([C_2H_2], ϕ, τ). However, the correlation between the contours of [C_2H_2] and T is -0.85 (*i.e*., weak orthogonality) (see Appendix). Therefore, S_2*([C_2H_2], ϕ, τ) is preferable. In order to investigate the validity of this choice of the variables of S_2*, the THCC matrices between [C_2H_2] and ϕ with the experimental measurement and the SVF predicted by the current soot model are compared (see Figs. 15 (a) and (b)). It is confirmed that the current soot model does not capture the THCC especially for the region $\phi < 2.0$, where the very strong correlation (=0.75) is observed in the THCC with the experimental data. This result suggests that S_2*([C_2H_2], ϕ, τ) might be a good candidate for modifying the current soot model in terms of the acetylene-based surface growth.

Region 2: 1000 [K] < T < 1200 [K] and 3.5 < ϕ

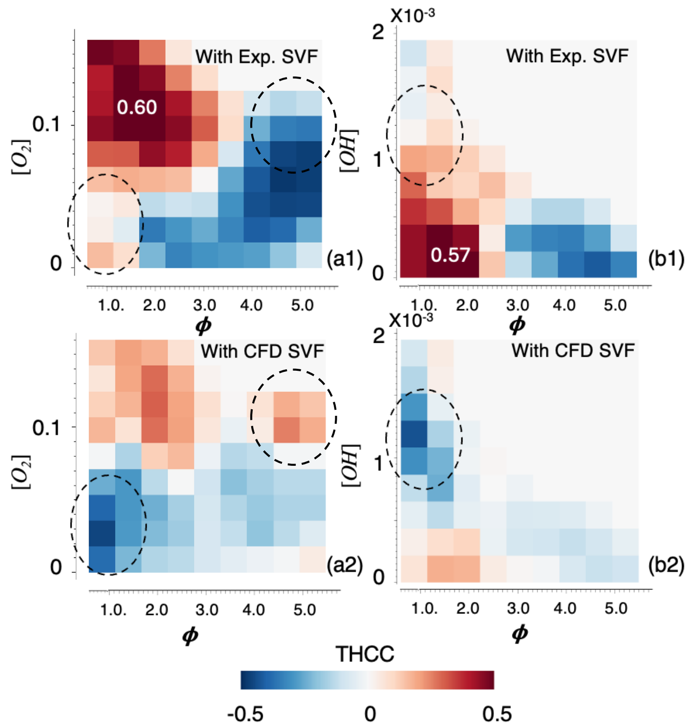

FIGURE 17: THCC MATRICES OF (left) [O_2] AND (right) [OH] WITH EQUIVALENCE RATIO USING (top) EXPERIMENTAL SVF AND (bottom) SVF CALCULATED BY THE SOOT MODEL

Although the soot model shows very weakly negative correlation in this low temperature, fuel-rich region, the difference between two plots is significant and the current soot models needs to be improved. This very fuel rich region seems to be associated with the PAH-based growth (e.g., see [33]). Since the PAH species are not included in the current 75 species mechanism, the model inadequacy in this very fuel rich region is to be expected. To mimic the PAH-based growth for this region, [C_6H_5], which is a precursor for the growth of PAH species, seems to be a reasonable choice of variable to construct the function, S_{PAH}*. Please note that S_{PAH}* would be a new function for the acetylene-based two equation model (not a modification for S_1 or S_2). Selection of the variables for S_{PAH}* needs to be performed with care, and the following three combinations: S_{PAH}*([C_6H_5], T, τ), S_{PAH}*([C_6H_5], ϕ, τ), and S_{PAH}*([C_6H_5], [C_2H_2], τ) are investigated.

An analysis was conducted by comparing the THCC matrices with respect to experimental SVF and the CFD predicted SVF for all three combinations, *i.e.* [C_6H_5] + T, [C_6H_5]+ϕ, and [C_6H_5]+[C_2H_2]. The resulting THCC matrices between [C_6H_5] and [C_2H_2] are shown in Figs. 16 (a) and (b). The THCC maps of [C_6H_5] + T and [C_6H_5]+ϕ are not shown here since the choice of [C_6H_5] and [C_2H_2] was found to be the more favorable option. As expected, the current soot model inaccurately captures the time-history effect in the majority of the ranges of [C_6H_5] and [C_2H_2]. This is a good indication that adding S_{PAH}*([C_6H_5], [C_2H_2], τ) as an additional nucleation source term could improve the current soot model.

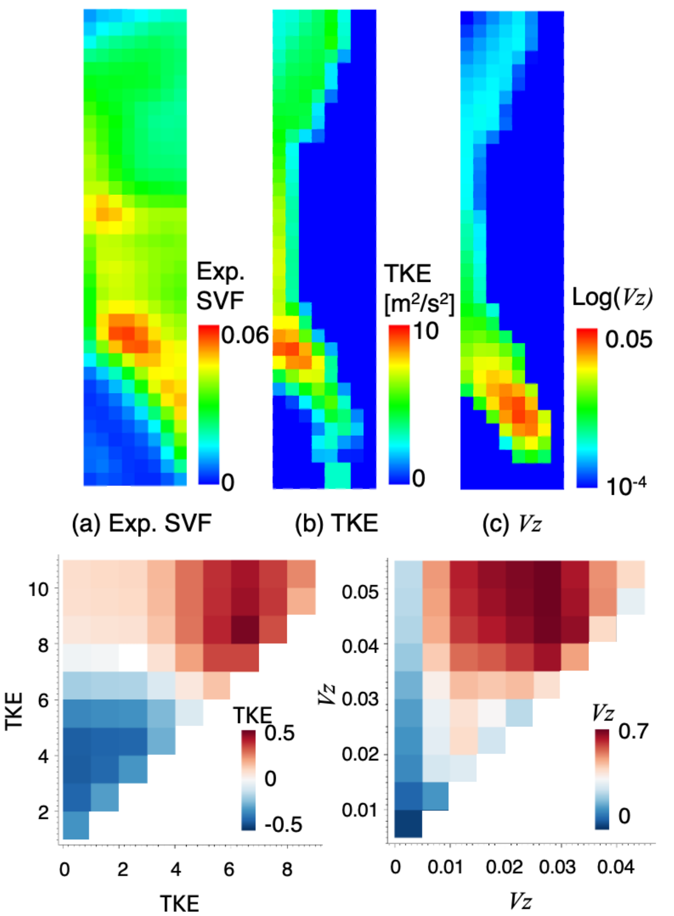

FIGURE 18: PARTICLE-BASED AVERAGED CONTOURS OF TKE AND LOG(Vz) AND THCC MATRICES OF TKE AND Vz WITH THE EXPERIMENTAL SVF DATA

Region 3: 1600 [K] < *T* and ϕ < *1.5*

Finally, the discrepancy seen in the hot fuel-lean region in Fig. 14 could be associated with the model inadequacy of the current oxidation term, S_3, which does not include any time-history effect. We adapt a similar process as for region 1 and region 2, to select the variables of the modified function of S_3*, and examine three possible combinations: $[O_2]+T$, $[O_2]+\phi$, $[OH]+T$, and $[OH]+\phi$. The correlation between $[O_2]$ and T is -0.91, and the that between $[OH]$ and T is 0.94. Due to the weak orthogonality, the combinations of $[O_2]+T$ and $[OH]+T$ are ruled out (see Appendix). Comparison of the THCC matrices with the experimental SVF and the CFD predicted SVF for the two remaining combinations of $[O_2]+\phi$ and $[OH]+\phi$.was performed (see fig 17). The left and right columns of Figs. 17 show the results of $[O_2]+\phi$ and $[OH]+\phi$, respectively. For the case with $[O_2]+\phi$, it is found that the current model fails to predict the time-history effect, especially in two regions: $[O_2] < 0.07$ and $\phi < 1.5$, and $[O_2] < 0.1$ and $\phi > 4.5$. The former location corresponds to the downstream region of the V-shape soot formation along the shear layer ($y > 0.04$ [m]), and the latter region is the very fuel

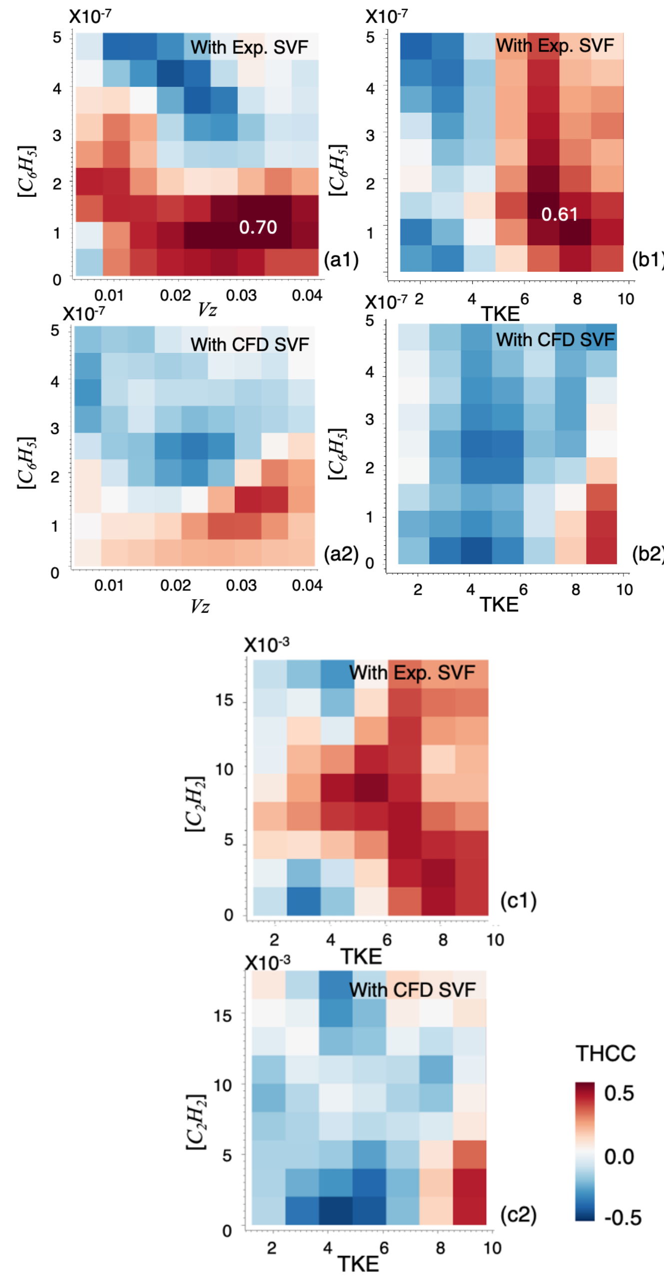

FIGURE 19: THCC MATRICES BETWEEN [C6H5] VS. Vz, [C6H5] VS. TKE, AND [C2H2] VS. TKE USING THE EXPERIMENTAL DATA AND THE PREDICTED SVF

rich upstream region. For $[OH]+\phi$, the model also fails in the region of $[OH] < 1\times10^{-3}$ and $\phi < 1.5$, which is close to the region of $[O_2] < 0.07$ and $\phi < 1.5$. Since $[O_2]$ and $[OH]$ are strongly correlated to each other (See Appendix), it is expected to see overlap in regions where the current semi-empirical model fails to predict the correct oxidation trend. Duvvuri, et al [45] reported that the soot disappears in the lean mixture region due to "spurious oxidation" and emphasized the important of model accuracy of the oxidation process in the lean region. Our analysis confirms that S_3*($[O_2]$, ϕ, τ) and S_3**($[OH]$, ϕ, τ) should be added into the oxidation model for better overall soot prediction in the lean region and very fuel rich region.

Discussion of Turbulent Effect on Soot Prediction

There has been active research about turbulence-chemistry-soot interactions (TCSI) in the context of LES (*e.g.*, [45, 46]). Even though the development of a subfilter model for the TCSIs is out of the scope of this study, it is worth checking whether or not the THCC approach can identify the importance of the time-history effect on the soot formation in terms of TCSIs. Figure 18 depicts the contours of the turbulent kinetic energy (TKE), *Vz,* and the THCC matrices of TKE and *Vz* generated with respect to the experimental data.

The very strong correlations seen in the THCC matrices implies that there is a favorable condition of turbulent intensity for the TCSIs through the time-history effect. The THCC analysis also provides further insights about how to incorporate the effects of turbulence time-history into the soot model.

Selected results are shown in Fig.19. For instance, comparing Fig. 19 (a1) and Fig.19 (a2), there is a reasonable agreement despite the fact that the magnitudes of the THCC for some ranges are slightly different. However, when considering the THCC matrices of [C_6H_5]+TKE using the experimental data and the calculated SVF (see Figs. 19 (b1) and (b2)), the current soot model does not capture well the trend in the region of TKE > 5.0. This might suggest that adding TKE as an additional variable of S_{PAH}*([C_6H_5], [C_2H_2], TKE, τ) could further improve the soot predictions in fuel-rich, high-nucleation regions of the combustor. An additional influence of TKE on soot nucleation is observed in the THCC matrices of [C_2H_2]+ TKE (see Fig. 19 (c1) and (c2)).

The effect of TKE on soot formation is not well captured by the current model in a majority of the parameter space (Fig 19 (c2), which strongly indicates that TKE should be incorporated into the role of [C_2H_2] as it relates to the proposed surface growth source term, i.e. S_2*.

CONCLUSIONS AND FUTURE WORK

The time-history effect in the context of soot formation was investigated with a particle-based statistical approach using the DLR aero-combustor. Large eddy simulation was conducted while injecting 10,000 massless tracers collecting time-history statistics of solution variables. Time-history statistics (e.g., time-history correlation coefficient or THCC) were then calculated with respect to the experimental soot volume fraction data acquired by Geigle *et al.* [1]. As part of the current work, we confirmed that time-history effects of certain flow variables, including turbulent quantities, and multiple species are indeed important for soot formation. The THCC with respect to experimental soot data, when combined with correlation coefficients among the particle-averaged solutions of a set of select species, helped identify certain key species (O_2, OH, C_2H_2, and C_6H_5) that could have significant impact on improving the current acetylene-based semi-empirical model of Fairweather *et al.* [24].

The particle-data collected in this work was also used to create two sets of THCC matrices, which were compared each other: Set A was computed with respect to the experimental SVF data and Set B was computed with respect to CFD predicted SVF profiles. Direct comparison of the two sets helped identify possible combinations of variables (including turbulent kinetic energy) that can be used to design functions to improve predictions of (a) C_6H_5-based nucleation in fuel-rich regions, (b) acetylene-based surface growth, and, (c) oxidation source terms related to OH and O_2 species.

The current work presents a novel approach towards demonstrating the viability of using a time-history based statistical approach for improving the CFD predictions of soot formation and oxidation for engineering applications. The time-history based soot modeling concept studied in this work is general enough that it can be applied independently of chemical kinetics, soot models, and gas-turbine combustor designs. In future work, the proposed modeling improvements will be tested for soot predictuons in the DLR combustor, and extended to other sets of experimental data available in the literature. The current work shows that time-history based modifications can provide a feasible path towards improving the accuracy of current engineering tools for CFD prediction of soot formation in gas-turbine combustors.

ACKNOWLEDGEMENTS

This research was funded by the Commercial Supersonic Technology (CST) Project under NASA's Advanced Air Vehicles Program (AAVP), and the Transformational Tools and Technologies (TTT) Project under NASA's Transformative Aeronautics (TAC) Program. Computational resources were provided by NAS Supercomputing at NASA Ames Research Center.

APPENDIX

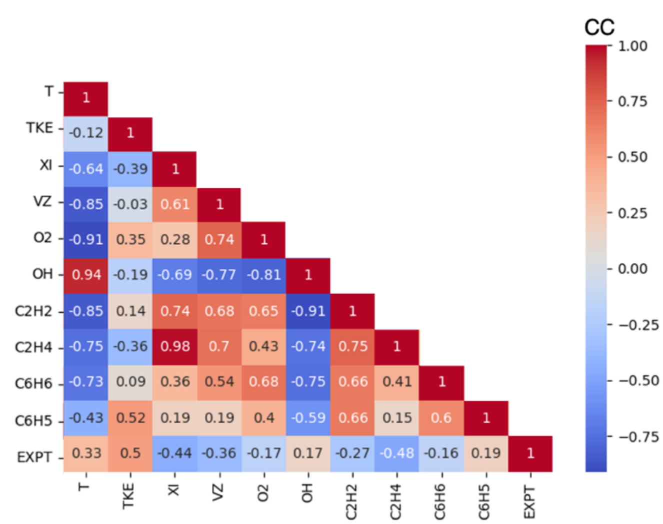

FIGURE A1: CORRELATION COEFFICIENT MATRIX

REFERENCES

[1] Peter Geigle, K., Hadef, R., and Meier, W., 2014, "Soot Formation and Flame Characterization of an Aero-Engine Model Combustor Burning Ethylene at Elevated Pressure," Journal of Engineering for Gas Turbines and Power, 136(2).
[2] Russell, A. G., and Brunekreef, B., 2009, "A focus on particulate matter and health," Environ Sci Technol, 43(13), pp. 4620-4625.
[3] Han, D., Chen, R., Kan, H., and Xu, Y., 2023, "The bio-distribution, clearance pathways, and toxicity mechanisms of ambient ultrafine particles," Eco Environ Health, 2(3), pp. 95-106.
[4] Ballal, D., DeWitt, M., Corporan, E., and Harrison, W., "Particulate Loading and Radiation in Gas Turbine Combustors," Proc. 41st Aerospace Sciences Meeting and Exhibit, AIAA 2003-337.
[5] Liu, F., Consalvi, J.-L., and Nmira, F., 2022, "The importance of accurately modelling soot and radiation coupling in laminar and laboratory-scale turbulent diffusion flames," Combustion and Flame, 258(1).
[6] Tewarson, A., 2004, "Combustion efficiency and its radiative component," Fire Safety Journal, 39(2), pp. 131-141.
[7] Stöhr, M., Geigle, K. P., Hadef, R., Boxx, I., Carter, C. D., Grader, M., and Gerlinger, P., 2019, "Time-resolved study of transient soot formation in an aero-engine model combustor at elevated pressure," Proceedings of the Combustion Institute, 37(4), pp. 5421-5428.
[8] Litvinov, I., Yoon, J., Noren, C., Stöhr, M., Boxx, I., and Geigle, K. P., 2021, "Time-resolved study of mixing and reaction in an aero-engine model combustor at increased pressure," Combustion and Flame, 231.
[9] Koo, H., Hassanaly, M., Raman, V., Mueller, M. E., and Peter Geigle, K., 2017, "Large-Eddy Simulation of Soot Formation in a Model Gas Turbine Combustor," Journal of Engineering for Gas Turbines and Power, 139(3).
[10] Grader, M., Yin, Z., Geigle, K. P., and Gerlinger, P., 2021, "Influence of flow field dynamics on soot evolution in an aero-engine model combustor," Proceedings of the Combustion Institute, 38(4), pp. 6421-6429.
[11] Franzelli, B., Tardelli, L., Stöhr, M., Geigle, K. P., and Domingo, P., 2023, "Assessment of LES of intermittent soot production in an aero-engine model combustor using high-speed measurements," Proceedings of the Combustion Institute, 39(4), pp. 4821-4829.
[12] Franzelli, B., Scouflaire, P., and Candel, S., 2015, "Time-resolved spatial patterns and interactions of soot, PAH and OH in a turbulent diffusion flame," Proceedings of the Combustion Institute, 35(2), pp. 1921-1929.
[13] Lee, S.-Y., Turns, S. R., and Santoro, R. J., 2009, "Measurements of soot, OH, and PAH concentrations in turbulent ethylene/air jet flames," Combustion and Flame, 156(12), pp. 2264-2275.
[14] Bisetti, F., Blanquart, G., Mueller, M. E., and Pitsch, H., 2012, "On the formation and early evolution of soot in turbulent nonpremixed flames," Combustion and Flame, 159(1), pp. 317-335.
[15] Rodrigues, P., Franzelli, B., Vicquelin, R., Gicquel, O., and Darabiha, N., 2018, "Coupling an LES approach and a soot sectional model for the study of sooting turbulent non-premixed flames," Combustion and Flame, 190, pp. 477-499.
[16] Maldonado Colmán, H., Attili, A., and Mueller, M. E., 2024, "Large Eddy Simulation of the evolution of the soot size distribution in turbulent nonpremixed flames using the Bivariate Multi-Moment Sectional Method," Combustion and Flame, 265, p. 113496.
[17] Wang, Q., Elvati, P., Kim, D., Johansson, K. O., Schrader, P. E., Michelsen, H. A., and Violi, A., 2019, "Spatial dependence of the growth of polycyclic aromatic compounds in an ethylene counterflow flame," Carbon, 149, pp. 328-335.
[18] Saldinger, J. C., Elvati, P., and Violi, A., 2021, "Stochastic and network analysis of polycyclic aromatic growth in a coflow diffusion flame," Phys Chem Chem Phys, 23(7), pp. 4326-4333.
[19] Attili, A., Bisetti, F., Mueller, M. E., and Pitsch, H., 2014, "Formation, growth, and transport of soot in a three-dimensional turbulent non-premixed jet flame," Combustion and Flame, 161(7), pp. 1849-1865.
[20] Michelsen, H. A., Colket, M. B., Bengtsson, P. E., D'Anna, A., Desgroux, P., Haynes, B. S., Miller, J. H., Nathan, G. J., Pitsch, H., and Wang, H., 2020, "A Review of Terminology Used to Describe Soot Formation and Evolution under Combustion and Pyrolytic Conditions," ACS Nano, 14(10), pp. 12470-12490.
[21] Saito, K., Gordon, A. S., Williams, F. A., and Stickle, W. F., 1991, "A Study of the Early History of Soot Formation in Various Hydrocarbon Diffusion Flames," Combustion Science and Technology, 80(1-3), pp. 103-119.
[22] Valencia, S., Ruiz, S., Manrique, J., Celis, C., and Figueira da Silva, L. F., 2021, "Soot modeling in turbulent diffusion flames: review and prospects," Journal of the Brazilian Society of Mechanical Sciences and Engineering, 43(4).
[23] Rigopoulos, S., 2019, "Modelling of Soot Aerosol Dynamics in Turbulent Flow," Flow, Turbulence and Combustion, 103(3), pp. 565-604.
[24] Fairweather, M., Jones, W. P., and Lindstedt, R. P., 1992, "Predictions of Radiative Transfer from a Turbulent Reacting Jet in a Cross-Wind," Combustion and Flame, 89, pp. 45-63.
[25] Frenklach, M., 2002, "Method of moments with interpolative closure," Chemical Engineering Science, 57, pp. 2229 – 2239.
[26] Marchisio, D. L., and Fox, R. O., 2005, "Solution of population balance equations using the direct quadrature method of moments," Journal of Aerosol Science, 36(1), pp. 43-73.
[27] Yuan, C., and Fox, R. O., 2011, "Conditional quadrature method of moments for kinetic equations," Journal of Computational Physics, 230(22), pp. 8216-8246.
[28] Mueller, M. E., Blanquart, G., and Pitsch, H., 2009, "Hybrid Method of Moments for modeling soot formation and growth," Combustion and Flame, 156(6), pp. 1143-1155.

[29] Chong, S. T., Raman, V., Mueller, M. E., Selvaraj, P., and Im, H. G., 2019, "Effect of soot model, moment method, and chemical kinetics on soot formation in a model aircraft combustor," Proceedings of the Combustion Institute, 37(1), pp. 1065-1074.
[30] Gelbard, F., Tambour, Y., and Seinfeld, J., 1980, "Sectional Representations for Simulating Aerosol Dynamics," Journal of Colloid and Interface Science, 76(2), pp. 541-556.
[31] Blacha, T., Di Domenico, M., Gerlinger, P., and Aigner, M., 2012, "Soot predictions in premixed and non-premixed laminar flames using a sectional approach for PAHs and soot," Combustion and Flame, 159(1), pp. 181-193.
[32] Dittmann, T., Fiolitakis, A., Gerlinger, P. M., and Aigner, M., 2019, "Simulation of a Piloted Turbulent Sooting Jet-Flame using a Transported-PDF and a Sectional Soot Modeling Approach," AIAA Scitech 2019 Forum.
[33] Chong, S. T., Hassanaly, M., Koo, H., Mueller, M. E., Raman, V., and Geigle, K.-P., 2018, "Large eddy simulation of pressure and dilution-jet effects on soot formation in a model aircraft swirl combustor," Combustion and Flame,192, 452-472.
[34] Colman, H. M., and Mueller, M. E., 2025, "Large Eddy Simulation of the evolution of the soot size distribution in turbulent nonpremixed bluff body flames," Combustion and Flame, 279, p. 114282.
[35] Ajmani, K., Guzman, F. J., and Miki, K., 2025, "CFD Evaluation of Soot Formation in a Gas Turbine Combustor Using a Flamelet Progress Variable Approach," Proceedings of the ASME Turbo Expo Memphis, Tennessee.
[36] Chong, S. T., Raman, V., Mueller, M. E., and Im, H. G., 2018, "The Role of Recirculation Zones In Soot Formation In Aircraft Combustors," Proceedings of ASME Turbo Expo 2018.
[37] Shih, T.-H., and Liu, N.-S., 2007, "Modeling of Internal Reacting Flows and External Static Stall Flows Using RANS and PRNS," Flow, Turbulence and Combustion,81(1), 279-299.
[38] Zambon, A. C., Muralidharan, B., Hosangadi, A., and Ajmani, K., 2020, "A Multi-Time-Scale Flamelet Progress Variable Approach in OpenNCC for Predicting NOx Applied to Commercial Supersonic Transport Combustor Designs," AIAA Propulsion and Energy 2020 Forum.
[39] Muralidharan, B., Zambon, A. C., Hosangadi, A., and Calhoon, W., 2018, "Application of a progress variable based approach for modeling non-premixed/partially premixed combustion under high-pressure conditions," 2018 Joint Propulsion Conference.
[40] Lueng, K. M., and Lindstedt, R. P., 1995, "Detailed kinetic modeling of C1 — C3 alkane diffusion flames," Combustion and Flame, 102(1-2), pp. 129-160.
[41] Liu, F., Guo, H., Smallwood, G., and Gülder, Ö. L., 2003, "Numerical modelling of soot formation and oxidation in laminar coflow non-smoking and smoking ethylene diffusion flames," Combustion Theory and Modelling, 7(2), pp. 301-315.
[42] Kennedy, I. M., Yam, C., Rapp, D. C., and Santoro, R. J., 1996, "Modeling and Measurements of Soot and Species in a Laminar Diffusion Flame," Combustion and Flame, 107, pp. 368-382.
[43] Franzelli, B., Riber, E., Cuenot, B., and Ihme, M., 2015, "Numerical modeling of soot production in aero-engine combustors using large eddy simulations," Proceedings of the ASME Turbo Expo 2015Montreal, Canada.
[44] Wang, H., and Frenklach, M., 1997, "A Detailed Kinetic Modeling Study of Aromatics Formation in Laminar Premixed Acetylene and Ethylene Flames," Combustion and Flame, 110, pp. 173-221.
[45] Duvvuri, P. P., Maldonado Colmán, H., and Mueller, M. E., 2022, "Relative influence of soot oxidation kinetics and subfilter soot-turbulence interactions on soot evolution in turbulent nonpremixed flames," Proceedings of the Combustion Institute, 39(1), pp. 959-967.
[46] Han, W., Raman, V., Mueller, M. E., and Chen, Z., 2019, "Effects of combustion models on soot formation and evolution in turbulent nonpremixed flames," Proceedings of the Combustion Institute, 37(1), pp. 985-992.
[47] Frenklach, M., and Mebel, A. M., 2020, "On the mechanism of soot nucleation," Phys Chem Chem Phys, 22(9), pp. 5314-5331.
[48] Semenikhin, A. S., Savchenkova, A. S., Chechet, I. V., Matveev, S. G., Frenklach, M., and Mebel, A. M., 2020, "On the mechanism of soot nucleation. II. E-bridge formation at the PAH bay," Phys Chem Chem Phys, 22(30), pp. 17196-17204.
[49] Frenklach, M., Semenikhin, A. S., and Mebel, A. M., 2021, "On the Mechanism of Soot Nucleation. III. The Fate and Facility of the E-Bridge," J Phys Chem A, 125(31), 6789-6795.
[50] Martin, J. W., Salamanca, M., and Kraft, M., 2022, "Soot inception: Carbonaceous nanoparticle formation in flames," Progress in Energy and Combustion Science, 88.
[51] Bockhorn, H., D'Anna, A., and Sarofim, A. F., 2009, Combustion generated fine carbonaceous particles, Universitätsverlag Karlsruhe.
[52] Wang, H., 2011, "Formation of nascent soot and other condensed-phase materials in flames," Proceedings of the Combustion Institute, 33(1), pp. 41-67.
[53] Hansen, N., Yang, B., Braun-Unkhoff, M., Ramirez, A., and Kukkadapu, G., 2022, "Molecular-growth pathways in premixed flames of benzene and toluene doped with propyne," Combustion and Flame, 243.
[54] Chu, T. C., Buras, Z. J., Smith, M. C., Uwagwu, A. B., and Green, W. H., 2019, "From benzene to naphthalene: direct measurement of reactions and intermediates of phenyl radicals and acetylene," Phys Chem Chem Phys, 21(40), 22248-22258.
[55] Couch, D. E., Zhang, A. J., Taatjes, C. A., and Hansen, N., 2021, "Experimental Observation of Hydrocarbon Growth by Resonance-Stabilized Radical-Radical Chain Reaction," Angew Chem Int Ed Engl, 60(52), pp. 27230-27235.
[56] Johansson, K. O., Head-Gordon, M. P., Schrader, P. E., Wilson, K. R., and Michelsen, H. A., 2018, "Resonance-stabilized hydrocarbon- radical chain reactions may explain soot inception and growth," Science, 361(6406), pp. 997-1000.
[57] Najm, H. N., Paul, P. H., Mueller, C. J., and Wyckoff, P. S., 1998, "On the Adequacy of Certain Experimental Observables as Measurements of Flame Burning Rate," Combustion and Flame, 113(3), pp. 312-332.